Nonlinear Landau-Zener tunneling under higher-order dispersion

Y. Cao ● and T. F. Xu[*]

Hebei Key Laboratory of Microstructural Material Physics, School of Science, Yanshan University, Qinhuangdao 066004, China

We studied nonlinear Landau-Zener tunneling under the effect of higher-order dispersion, transformed the Gross-Pitaevskii (GP) equation with higher-order dispersion terms into a nonlinear two-energy level form using a two-mode approximation, and comprehensively analyzed the loop structure of the lowest-energy band and the nonlinear Landau-Zener tunneling. The results show that, when third-order dispersion coefficient is not zero, there is a spatial inversion symmetry breaking of the energy band structure and unbalanced Landau-Zener tunneling. By analyzing the fixed point's nature of the classical Hamiltonian, we obtain a law for the variation of the loop structure and adiabatic tunneling probability with the dispersion coefficient, consistent with our numerical analysis results. In addition, we analyzed the real-time evolution of solitons with transverse bias and observed the tunneling phenomenon. Consistent with our analysis, the adjustment of the dispersion term can effectively control optical tunneling, which provides an alternative idea for optical switching.

I. INTRODUCTION

The phenomenon of quantum tunneling is one of the most remarkable results in quantum mechanics, showing that particles can penetrate the classically forbidden zone and is the best proof of the fluctuating nature of particles, which can be found in the textbook on quantum mechanics. When the system is in an external potential well, symmetry breaking leads to splitting energy levels at the boundary of the Brillouin zone, forming tiny energy gaps where physical solutions are forbidden and tunneling does not occur in the adiabatic case. Wu *et al.* found that, as nonlinear intensity increases, there are loop structures in the lowest energy band [1]. The crossing of energy levels causes adiabatic tunneling to occur [2], a finding that immediately attracted widespread attention. Subsequently, people began a large number of studies on loop structures, which showed that in any external potential well background, as long as the nonlinear intensity is large enough, it gives rise to the loop structures [3,4] and numerically gave the conditions for the appearance of loop structures [5]. Then, based on the loop structure, the tunneling phenomenon [6,7] due to the loop structure was verified both theoretically and experimentally and extended to various applications, such as diode [8], waveguide arrays [9], solitons [10], and so on. Thereafter, a vast amount of literature was devoted to the study of nonlinear Landau-Zener (LZ) tunneling [6,11,12], in many recent studies, it is also called Landau-Zener-Stückelberg-Majorana (LZSM) tunneling [13–16]. In Bose-Einstein condensation (BEC), the possibility of applying various models has been extensively discussed [17], and the laws of variation of linear and nonlinear tunneling probabilities with parameters have been analyzed [18], laying the theoretical foundation for future practical applications.

Recently, Blanco Redondo *et al.* discovered pure quartic solitons (PQS) [19] in silicon photonic crystal waveguides. This soliton exists in the equilibrium of anomalous fourth-order dispersion and Kerr nonlinearity. The team suggested the possibility of pure quartic soliton lasers [20], which led to a wide discussion of higher-order dispersions. Literature [21] shows that the combination of second- and fourth-order dispersion may improve the performance of soliton lasers. In addition, the soliton dynamics under second-, third- and fourth-order dispersions were analyzed [22]. These studies showed that higher-order dispersion can no longer be considered a perturbation but plays an important role. Of course, studying nonlinear LZSM tunneling under higher-order dispersion is also necessary.

In the present paper, we consider the common two-energy level systems and study the nonlinear LZSM tunneling phenomenon under the effect of higher-order dispersion. We predict the effect of each dispersion term on the loop structure by analyzing the nature of the fixed points in the phase space of the classical Hamiltonian system. We show analytically that the lowest energy band shows a complex loop structure due to the dissipative effect of third-order dispersion. Interestingly, the nonlinear LZSM tunneling exhibits nonreciprocity in different sweep directions due to the spatial inversion symmetry breaking by the dissipation. We reveal the physical mechanism behind this phenomenon. We also discuss the possible numerical simulation observation of our results with gap solitons in optical lattices under transverse bias, giving the possibilities of this model in practical applications.

The paper is structured as follows. In Sec. II, we introduce the nonlinear Schrödinger equation under higher-order dispersion, which can be described by a GP-like equation. And under the two-mode approximation, we transform it into a nonlinear two-energy level model and obtain its corresponding classical Hamiltonian. Then we give the adiabatic energy level, which is consistent with the results of the fixed point

_____
[*]tfxu@ysu.edu.cn

stability analysis. In Sec. III, we investigate the loop structure by analyzing the fixed points in phase space to find the loop structure pattern for different dispersion coefficients. Section IV studies in detail the variation of the nonlinear LZSM tunneling probability with different parameters. In Sec. V, we consider the evolution of fundamental gap solitons under transverse bias, which gives the possibility of application in the optics. We have conclude in Sec. VI.

II. MODEL

In this paper, we consider the case of optical wave propagation in a Kerr nonlinear periodic potential with higher-order dispersion under the action of external transverse bias, where the beam propagating is described by the following dimensionless generalized Schrödinger-like equation [19,23,24]

$$i\frac{\partial \psi}{\partial z} = -\frac{\beta_2}{2}\frac{\partial^2 \psi}{\partial x^2} - i\frac{\beta_3}{6}\frac{\partial^3 \psi}{\partial x^3} + \frac{\beta_4}{24}\frac{\partial^4 \psi}{\partial x^4}$$
$$+ v_0\cos(x)\psi - \beta x\psi + c|\psi|^2\psi. \quad (1)$$

Here, ψ is the dimensionless amplitude of the beam, x and z are generalized coordinates. In optical fibers, z represents the direction of propagation and x represents the retarded time. Their units are mm and ps, respectively. The parameter β_i indicates the ith-order dispersion coefficient described by $\partial^i K/\partial \omega^i$ and its units are $ps^i mm^{-1}$ throughout this paper. Here, K is used to distinguish it from k in the following paper to represent light wave numbers. The βx denotes the external transverse bias and β represents the strength of the bias. In practical applications, we can control our sweep rate by varying the intensity of the transverse bias. c is the Kerr nonlinearity coefficient and its units is $W^{-1}mm^{-1}$ which is the same as v_0. The plus-minus sign characterizes the type of nonlinearity, defocusing (or repulsion), when c is greater than zero and focusing (or attraction) when c is less than zero. When v_0 is sufficiently small, the lowest two bands are very close to each other and far away from other bands near the boundary of the Brillouin zone $k_{BZ} = 1/2$, LZSM tunneling is more likely to occur here. To capture this tunneling effect analytically, we apply a two-mode approximation here in which the plane wave is decomposed into the two modes at the boundary and the higher modes are ignored. That is,

$$\psi(x, z) = a_1(z)\exp[ik(z)x] + a_2(z)\exp[i(k(z) - 1)x], \quad (2)$$

where a_1 and a_2 denote the amplitudes of the two plane-wave components, according to the normalization condition, the two variables are required to satisfy $|a_1(z)|^2 + |a_2(z)|^2 = 1$ and $k(z)$ denotes the Bloch wave vector. Due to the external transverse bias, $k(z)$ is no longer a constant but a function of z. For the convenience of calculation, we define the term $dk/dz = \beta$ in the derivation of the two-energy level model since the transverse bias can always be adjusted appropriately such that this definition is satisfied. After bringing the two-mode approximation into Eq. (1) and performing algebraic operations [25,26], we obtain a nonlinear two-energy level equation

$$i\frac{\partial}{\partial z}\begin{pmatrix}a\\b\end{pmatrix} = \begin{pmatrix}L - c|a|^2 & \frac{v_0}{2}\\ \frac{v_0}{2} & -L - c|b|^2\end{pmatrix}\begin{pmatrix}a\\b\end{pmatrix} = H(\gamma)\begin{pmatrix}a\\b\end{pmatrix}. \quad (3)$$
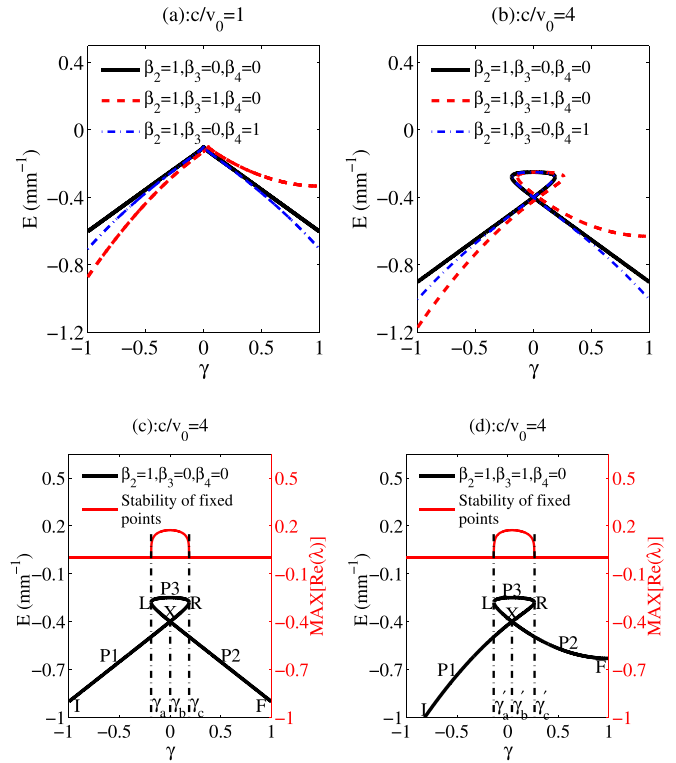
FIG. 1. Adiabatic energy levels and stability of fixed points $v_0 = 0.1$. (a,b) denote the lowest energy level at different nonlinear constants. (c,d) P_i ($i = 1, 2, 3$) is the fixed point of the classical Hamiltonian H_c system whose corresponding trajectories are $P1 \rightarrow IXR$, $P2 \rightarrow LXF$, $P3 \rightarrow LR$. L and R are the left and right limits of the loop, respectively, and X corresponds to the energy-level crossing point.

This two-energy level model has the same form as in Ref. [1] when third- and fourth-order dispersion coefficients are zero. In Eq. (3), we have

$$L = \frac{\beta_2}{2}\alpha z - \frac{\beta_3}{6}\left(\frac{3}{2}\alpha^2 z^2 + \frac{1}{8}\right) + \frac{\beta_4}{24}\left(2\alpha^3 z^3 + \frac{1}{2}\alpha z\right). \quad (4)$$

In numerical studies, we take $k(z) = 1/2 + \alpha z$. In addition, α is called the sweep rate, its magnitude is related to the external transverse bias strength β. When α is equal to zero it denotes an adiabatic process, namely, $\beta = 0$. We want to study nonlinear LZSM tunneling, that is, how the system evolves in the z direction for different sweep rates. For simplicity, we define $\gamma = \alpha z$. We can obtain our nonlinear adiabatic energy levels $E(\gamma)$ by solving Eq. (3) through diagonalizing the Hamiltonian $H(\gamma)$, see Fig. 1. It can be seen that, no matter how the dispersion coefficient varies, the top of the energy band is sharply pointed when $c = v_0$. Here it can be considered as the limiting case where the width of the loop structure is zero and the width of the loop gradually increases as c increases, which is consistent with the results of Ref. [2]. In Fig. 1(b), it can be seen that the change in fourth-order dispersion coefficient has a particularly small effect on the loop structure, but the change in the energy band outside the loop is particularly pronounced. As the fourth-order dispersion coefficient increases, the energy band gradually decreases, corresponding to an increase in the width of the energy band. When the

third-order dispersion coefficient is not zero, the energy band is no longer symmetric, which corresponds to our Hamiltonian's spatial inversion symmetry breaking, namely, $E(k) \neq E(-k)$. It is well known that, in nonlinear two-energy systems, the loop structure represents adiabatic nonlinear LZSM tunneling. When spatial symmetry is broken, tunneling probabilities are inconsistent under different sweep directions (α in the case of different signs), resulting in unbalanced LZSM tunneling. This phenomenon is referred to in Ref. [27] as nonreciprocal LZSM tunneling and an exact numerical verification is given.

To better understand this interesting phenomenon, we consider an equivalent classical Hamiltonian where the nonzero adiabatic tunneling probability is considered as a consequence of collisions between fixed points [1]. We define $a = |a|e^{i\theta_a}$, $b = |b|e^{i\theta_b}$, and let $\theta = \theta_b - \theta_a$, $s = |b|^2 - |a|^2$. s and θ are a pair of canonical variables in a classical Hamiltonian system [28] satisfying $\frac{ds}{dz} = -\frac{\partial H_c}{\partial \theta}$, $\frac{d\theta}{dz} = \frac{\partial H_c}{\partial s}$. The classical Hamiltonian is obtained by a simple calculation

$$H_c = -v_0\sqrt{1-s^2}\cos\theta + \beta_2\gamma s - \frac{\beta_3}{6}\left(3\gamma^2 s + \frac{1}{4}s\right)$$
$$+ \frac{\beta_4}{24}(4\gamma^3 s + \gamma s) + \frac{1}{2}cs^2. \tag{5}$$

It has the form of a Josephson Hamiltonian [29] whose fixed point is given by the following system of equations:

$$\frac{\partial H_c}{\partial \theta} = v_0\sqrt{1-s^2}\sin\theta = 0,$$
$$\frac{\partial H_c}{\partial s} = v_0\frac{s}{\sqrt{1-s^2}}\cos\theta + \beta_2\gamma - \frac{\beta_3}{6}\left(3\gamma^2 + \frac{1}{4}\right)$$
$$+ \frac{\beta_4}{24}(4\gamma^3 + \gamma) + cs = 0. \tag{6}$$

It can be obtained from the above Eq. (6) that the fixed point in a period only exists on the $\theta = 0, \pi$, and 2π. When the loop structure appears, the eigenstate that corresponds to the LR segment in Figs. 1(c) and 1(d) should be unstable, and as the sweep proceeds, the eigenstate at R cannot remain in its original state, the fixed point P3 corresponding to the classical Hamiltonian is also unstable, and we obtain the corresponding Hamilton-Jacobi matrix by linearizing the above set of equations near the fixed point

$$\begin{pmatrix} -\frac{\partial^2 H_c}{\partial\theta\partial s} & -\frac{\partial^2 H_c}{\partial\theta^2} \\ \frac{\partial^2 H_c}{\partial s^2} & \frac{\partial^2 H_c}{\partial s\partial\theta} \end{pmatrix}. \tag{7}$$

By studying the eigenvalues of this matrix, we can obtain the stability interval of the fixed point. When the real part of this eigenvalue (λ) is zero, the fixed point is stable. On the contrary, the fixed point is unstable [30], corresponding to the loop structure in our adiabatic energy level. By comparing the two methods, we obtain consistent results, as shown in Figs. 1(c) and 1(d), which also shows that the nature of the fixed point is closely related to the loop structure and even the nature of the nonlinear LZSM tunneling is closely linked. In the next section, we will discuss in detail the law of the fixed point with respect to the variation of the parameters.

III. CLASSICAL PHASE DIAGRAMS AND FIXED POINT ANALYSIS

First, we focus on the variation of the fixed point in phase space in relation to the adiabatic energy level. Figure 2 shows us the evolution of the phase space for different third-order dispersion coefficients. When γ evolves from negative to positive infinity, the adiabatic energy level before the L point in Fig. 1(c) corresponds to the fixed point P1 at the bottom of the phase space. At the L point, a doubly split fixed point appears at the top of the phase space, where the unstable fixed point P3 moves towards the bottom after the split. As can be seen from the phase diagram, at the R point ($\gamma = \gamma_c$), P1 collides with P3 and the two fixed points disappear, which means that adiabatic tunneling occurs [1]. The motion of P3 corresponds to the LR segment in the adiabatic energy level, while the R point represents the case where the fixed points collide exactly at the bottom. The other stable fixed point P2, after the split, then keeps moving towards the top until it finally reaches the top at $s = 1$ when $\gamma \to \infty$. At the same time, we observe that the energy level crossing point X corresponds to the case where P3 is exactly in the middle of the phase space ($s = 0$) and the entire phase diagram is symmetric up and down, see Figs. 2(a) to 2(d). The situation is also the same for the points corresponding to Fig. 1(d) and Figs. 2(e) to 2(h) when the third-order dispersion coefficient is not zero, but it can be observed that P3 does not reach $s = 0$ at $\gamma_b = 0$ when the third-order coefficient is not zero. This result represents the presence of third-order coefficients that lead to a shift in the loop structure, which is consistent with the spatial inversion symmetry breaking conclusions we observe. The offset of the loop structure is also discussed in another reference [18]. In summary, it can be seen that the unstable fixed point P3 characterizes all the features of the loop structure (L, R, X points). To better demonstrate the effect of different coefficients on P3, we analyzed the nature of the motion of P3 in phase space with different parameters, see Fig. 3.

Here we compare the s-γ diagram with the classical case of the s-t diagram (position-time diagram), where we assume that γ here characterizes "time" and s denotes the position of the fixed point in the phase diagram. By analyzing Eq. (3), it is found that the effect of the second- and fourth-order dispersion coefficient on the fixed point should be the same, so afterward, we only discuss the effect of the second- and third-order dispersion coefficient on the nature of the fixed point. Figure 3(a) shows that the "existence time" of P3 decreases as the second-order dispersion coefficient β_2 increases, which corresponds to a reduction in the width of the loop structure of our adiabatic energy level when other parameters are constant, that is, the increase of β_2 acts as a suppressor of the loop structure. However, it can be seen that, when the nonlinear constant c is determined, the positions s of the splitting and collision points corresponding to P3 do not change for different parameters and the absolute values of the two positions are equal. According to our previous conclusion, all the curves intersect at the point $(0, 0)$, which corresponds to the fact that the energy level crossing point X is all at $\gamma = 0$. The energy levels do not shift as β_2 and the nonlinear constant c change. In Fig. 3(b), we compare the evolution of each fixed point for different nonlinear constants. When $c > v_0$, the collision and
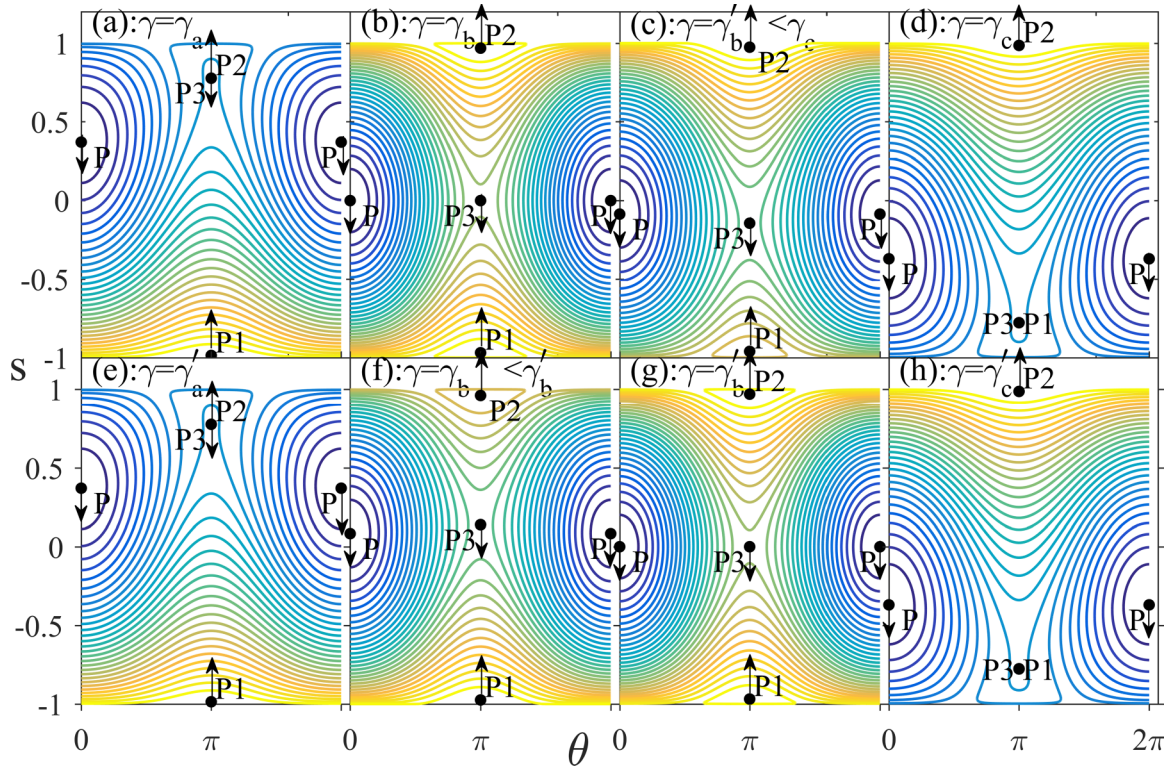
FIG. 2. Evolution of classical Hamiltonian in phase space and distribution of fixed points. The evolutionary process of (a)–(d) corresponds to Fig. 1(c) and (e)–(h) correspond to Fig. 1(d). Here, fixed point P corresponds to the eigenstate of the second energy level and the direction indicated by the arrow is the direction in which the fixed point moves as γ increases. In (d) and (h), $P1$ collides exactly with $P3$, after which the two fixed points disappear, implying that adiabatic LZSM tunneling has occurred.

splitting points move towards the two edges, respectively, as c increases, which represents an increase in the loop structure. At $c = v_0$, we can exactly see that both the collision and splitting points are at $s = 0$, which means that the fixed points just split and immediately collide, then disappear and c is in a critical position, while at $c < v_0$, neither splitting nor collision exists. Even in the case of an asymmetric loop structure, the curves intersect at the same point $(\gamma_b', 0)$ as long as the dispersion parameter does not change, which means that the offset of the adiabatic energy level is only related to the third-order dispersion coefficient. As β_3 increases, the entire loop structure moves in the positive direction of γ, the result is shown in Fig. 3(c). As shown in Fig. 3(d), the "velocity" of the entire fixed point decreases due to the presence of β_3. Moreover, the "velocity" at the split point is no longer the same as at the collision point. The third-order dispersion causes a decrease in velocity at collision. It can be predicted that as β_3 continues to increase, it may cause the "velocity" of $P3$ at collision to decrease to zero or even cause the reversal of $P3$. This phenomenon is because the third-order dispersion acts as a dissipation in the system. According to our analysis of the splitting point L, collision point R, and energy level crossing point X, as β_3 increases, the energy levels first shift, due to the "velocity" decrease, see Fig. 4(b). Following the increase of β_3 will cause $P3$ first collides with $P1$. Then $P3$ reverses and collides with $P2$, showing a double-loop structure in the center of the Brillouin zone, which is also mentioned in Refs. [31,32], see Fig. 4(c). Then, based on the before case, continuing to increase β_3, $P3$ reverses to collide with $P2$

before it gets to collide with $P1$, and the energy level exhibits the shape of a double-loop merger, see Fig. 4(d). It is worth noting that there is also a possibility of double-loop merging. On the basis of Fig. 4(c), that is, the double-loop appears case, we increase the nonlinear constant c, which will also lead to the generation of this phenomenon. The merger in this case is due to an increase in the width of the loop structure causing the two loops to collide, see Fig. 4(f). Finally, the increase of β_3 will cause the $P3$ point not to pass $s = 0$. In this case, the energy level crossover will not occur and the loop will be out of the lowest energy band, see Fig. 4(e). From the appearance of the double-loop structure, the adiabatic energy levels that follow all mean that eventually $P3$ will collide with $P2$ and the adiabatic tunneling will disappear.

IV. NONLINEAR LZSM TUNNELING

Due to the effect of nonlinearity, it is difficult to obtain an analytical expression for the nonlinear LZSM tunneling probability. To study this tunneling, we use numerical evolution to solve Eq. (3), the initial value of (a, b) at $\gamma \rightarrow -\infty$ is chosen to be $(1, 0)$, namely, at the beginning of the system, the particles are all in the lowest energy band. The tunneling probability is defined as the value of $|a|^2$ at $\gamma \rightarrow \infty$.

In this section, we focus on two cases of tunneling. One is tunneling in the adiabatic limit since, in a truly adiabatic state, the system will always be in the transient ground state and LZSM tunneling cannot occur, so we can only consider the near-adiabatic case [33], namely, $\alpha \rightarrow 0$. Here, we choose
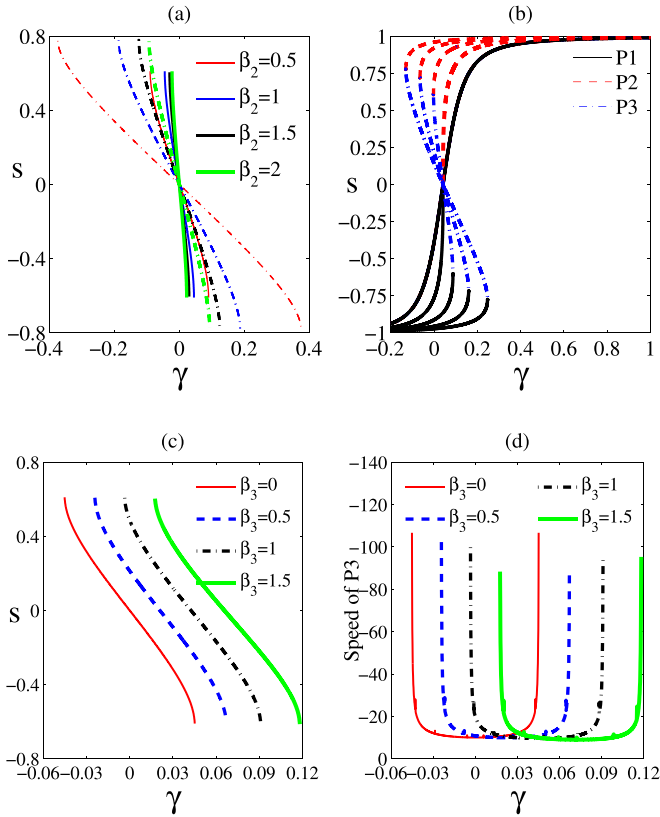
FIG. 3. Evolution of the position s of the fixed point in phase space with γ. (a) For the fixed point $P3$, the constant parameters are $\beta_3 = \beta_4 = 0$, $v_0 = 0.1$, the solid and dashed lines denote $c = 0.2$ and $c = 0.4$, respectively. (b) Looking at the $s > 0$ part, from left to right represents $c = 0.4, 0.3, 0.2, 0.1$, and 0, other parameters are $\beta_2 = \beta_3 = \beta_4 = 1$, $v_0 = 0.1$. (c) For the fixed point $P3$, the constant parameters are $\beta_2 = 1$, $\beta_4 = 0$, $c = 2v_0 = 0.2$. (d) Corresponds to the velocity at the fixed point under each parameter in Fig. 3(c).

$\alpha = 0.0001$ as the case of the adiabatic limit. In the adiabatic limit, the tunneling probability should be determined by the topology of the adiabatic energy level and the nature of the eigenstates, which corresponds to our analysis of the fixed point of the classical Hamiltonian system in Sec. III. In the previous section, we already know that the presence of third-order dispersion can lead to spatial inversion symmetry breaking and even double-loop structure can appear, which we also can see by the evolution of the number density of particles, see Fig. 5(a). When the third-order dispersion coefficient is small, the distribution of the number density of particles hardly changes. It just tends to be more difficult to stabilize at the same time. Moreover, as the third-order dispersion coefficient increases, the double-loop structure appears and the particles will make second transition. When continuing to increase the third-order dispersion coefficient, the double-loop structure becomes closer, signaling that the second transition of the particle will occur immediately after the first. This makes it difficult to distinguish between the two transitions, but eventually the particle will return to the ground state, which corresponds to the return of the fixed point $P3$ to collide with the top stable fixed point $P2$ in phase space. The larger the third-order dispersion coefficient, the faster
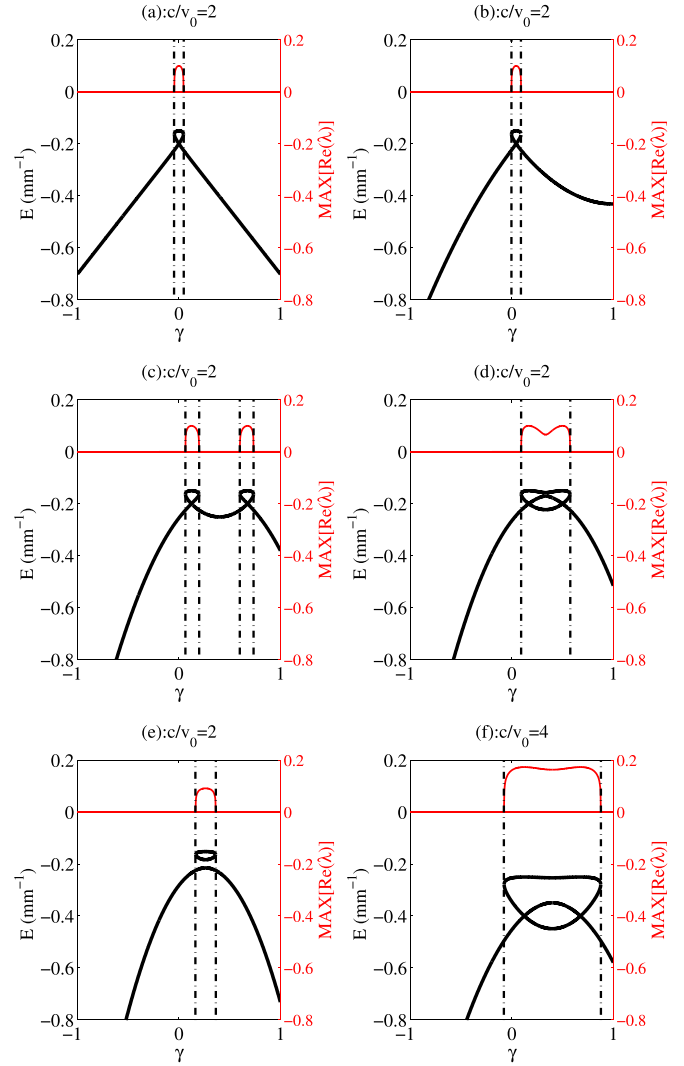
FIG. 4. Loop structure of the lowest energy band for different third-order dispersion coefficients. Thick black line indicates the adiabatic energy band and the thin red line indicates the stability analysis of the fixed points. The other invariant parameters are $v_0 = 0.1$, $\beta_2 = 1$, and $\beta_4 = 0$. (a) $\beta_3 = 0$; (b) $\beta_3 = 1$; (c) $\beta_3 = 2.5$; (d) $\beta_3 = 3$; (e) $\beta_3 = 3.8$; (f) $\beta_3 = 2.5$.
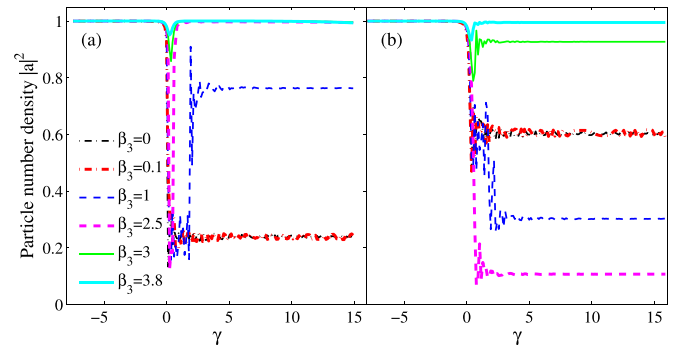
FIG. 5. Density distribution of particle number. The invariant parameters are $c = 2v_0 = 0.2$, $\beta_2 = 1$, and $\beta_4 = 0$. (a) $\alpha = 0.0001$; (b) $\alpha = 0.02$.
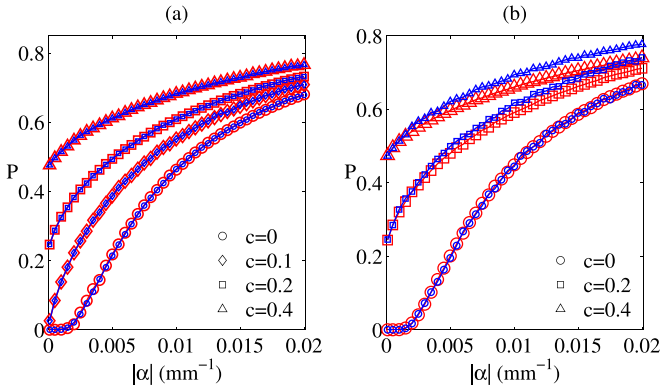
FIG. 6. Relationship between nonlinear LZSM tunneling probability and sweep rate α. Red (big symbol) for the forward sweep and blue (small symbol) for the reverse sweep. Here $v_0 = 0.1$, $\beta_2 = 2$, and $\beta_4 = 1$. (a) $\beta_3 = 0$; (b) $\beta_3 = 1$.

this process occurs, which is an inevitable consequence of the dissipative effect of third-order dispersion in the system. We will subsequently discuss the effect of this coefficient on the overall nonlinear LZSM tunneling. The second is the tunneling in general, where the particles will get energy from the outside due to transverse bias and more easily break through the Bragg reflection at the edge of the energy band into a higher energy state, see Fig. 5(b). We can see tunneling occurs under transverse bias. Even if it does not occur in adiabatic conditions, the particle number density distribution becomes more complex. Due to dissipative effects, the spatial inversion symmetry is broken and the tunneling probability should behave inconsistently in different bias directions, namely, in different sweep directions. It manifests itself as a result of the combined effect of dissipation and transverse bias and corresponds to the nonreciprocal LZSM tunneling mentioned earlier. To study this tunneling phenomenon, we define two sweep directions, forward sweep when $\alpha > 0$, that is, $\beta > 0$, and reverse sweep when the opposite is true. As shown in Fig. 6, when the third-order dispersion coefficient is zero, the probabilities of forward and reverse sweeps are the same and independent of the nonlinear coefficient, which manifests itself as our common tunneling. However, when the third-order coefficient is not zero the two will no longer be in agreement. Their difference becomes more pronounced as the nonlinear coefficient increases and transverse bias intensity but almost converges at near-adiabatic. To better investigate the nonreciprocal LZSM tunneling, we restricted the third-order dispersion coefficient to the case without double-loop structure because the presence of the double-loop structure will complicate the tunneling. From a physical point of view, it can be analyzed that the effect of transverse bias in the forward sweep provides energy for the particles to transition from a lower energy state to a higher energy state. In contrast, the effect of third-order dispersion is the opposite, so the presence of the third-order dispersion coefficient is predicted to reduce the tunneling probability. This conclusion is confirmed in Fig. 7(b). However, in the reverse sweep case, we consider the transition probability from a higher to a lower energy state. The third-order dispersion has the opposite effect to the first case, acting as a "gain," but in this case, it is constrained
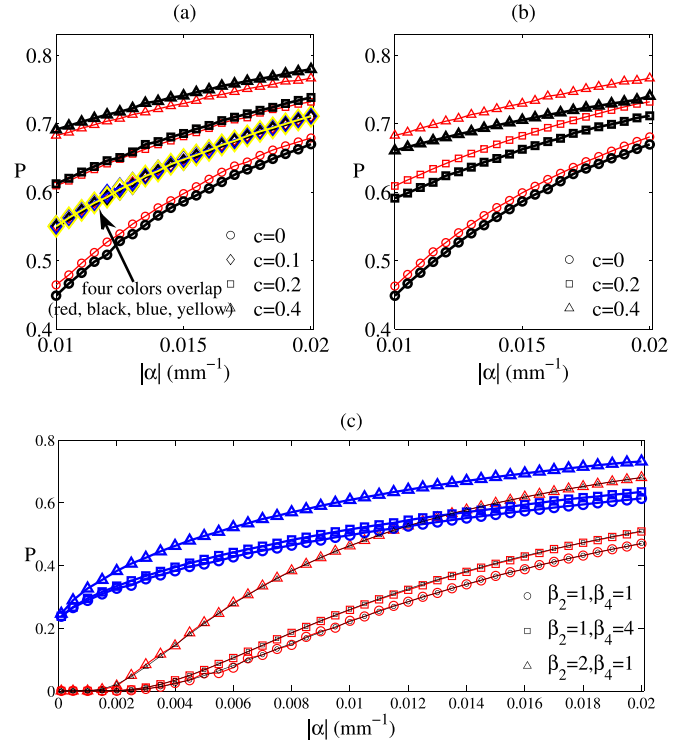
FIG. 7. Relationship between nonlinear LZSM tunneling probability and sweep rate α. $v_0 = 0.1$. (a,b) $\beta_2 = 2$, $\beta_4 = 1$. The red (thin) and black (thick) colors indicate the third-order dispersion coefficients $\beta_3 = 0$ and $\beta_3 = 2$, respectively. Here (a) for the reverse sweep, and in the $c = 0.1$ case, blue and yellow represent $\beta_3 = 1$ and $\beta_3 = 1.5$, respectively. (b) For the forward sweep. (c) $\beta_3 = 0$, black (small symbol), red (thin), and blue (thick) indicate the exact linear value, the numerical simulation results in the linear case, and in the $c = 2v_0$ case, respectively.

by nonlinear constants, as seen in Fig. 7(a). The presence of the third-order dispersion coefficient reduces the tunneling probability when the loop structure is absent. Nevertheless, at the critical value of the loop structure, namely, when $c = v_0$, the effect of the magnitude of the third-order coefficient on the tunneling probability is almost zero. To avoid chance we tested a variety of third-order dispersion coefficients in this case. The results show that this is a common situation and that the "gain" effect of third-order dispersion coefficients manifests itself as the loop structure emerges. The presence of third-order dispersion coefficients increases the tunneling probability. Since the third-order dispersion coefficient works differently on the tunneling probability in different sweep directions, this leads to the appearance of nonreciprocal tunneling. In addition, we are also interested in the effect of second- and fourth-order dispersion coefficients on the tunneling probability and when the third-order dispersion coefficient is zero, according to the Refs. [34,35], we obtain the linear tunneling probability of the system as follows:

$$P_L = e^{-\frac{\pi v_0^2}{2(\beta_2 + \beta_4/24)|\alpha|}}, \tag{8}$$

which is consistent with our numerical simulation results, see Fig. 7(c), we can see from the structure of Eq. (8) that, in this case, the tunneling is balanced and independent of the

sweep direction. Figure 7(c) shows that as second- and fourth-order dispersion coefficients increase, both contribute to the tunneling probability, except that the second-order dispersion is much more powerful than the fourth-order dispersion. In practice, we can use adjusting the second-order dispersion to achieve coarse-tuning and adjust the fourth-order dispersion to achieve more precise control. Furthermore, the effect of the two diminishes as the nonlinear constant increases. In the next section, we will discuss more specific cases and use simulations to prove our conclusions.

V. TUNNELING PHENOMENON OF SOLITONS

In the absence of an external transverse bias, we use the separation of variables method $\psi(x, z) = \phi(x) \exp(-i\mu z)$ for Eq. (1) to obtain a nonlinear Schrödinger equation independent of the z direction and then solve this equation by using Newton's iteration method to get the soliton solution.

We use the Crank-Nicolson method and the second-order time-splitting step method [36,37] to monitor the evolution of solitons in the z direction. We already concluded in the previous section that tunneling will occur when the strength of the transverse bias is sufficiently large. To observe the LZSM tunneling of solitons, we chose different bias strengths, see Fig. 8. First, we start with $\beta = 0$, which is the same as our known conclusion that solitons can maintain stable propagation. As β increases, we first observe the phenomenon of Bloch oscillations. This is due to the strength of the transverse bias not being sufficient to support the soliton breaking through the Bragg reflection at the edge of the first Brillouin zone, leading to the phenomenon of oscillations of the soliton in the Brillouin zone [38,39], see Figs. 8(a) and 8(b). The same phenomenon was mentioned in the literature [40]. Abdullaev *et al.* analyzed the Bloch oscillation phenomenon in the BEC system in detail through numerical analysis and simulation. They pointed out that, when the scattering length is positive, which corresponds to our case, the nonlinear constant c is greater than zero. The excitation generated on the BEC array can occur in Bloch oscillation when the initial pulse velocity is small but not zero. In our model, the external transverse bias is equivalent to adding an initial lateral velocity to the initial soliton wave and when $\beta = 0.1$, compared with stable propagation can be found that there is an obvious oscillation of Fig. 8(b). Then we continue to increase the bias strength and the soliton breaks through the edge of the first Brillouin zone, which shows in Fig. 8(c), oscillations are suppressed, and tunneling occurs [41]. In Figs. 8(c) and 8(d), it is shown that increasing the second-order dispersion coefficient makes tunneling more likely to occur when the transverse bias strength is given, signifying an increase in the tunneling probability. This can also be seen from the strength of the solitons that maintain straight-line propagation. The higher the tunneling probability, the weaker the strength that maintains straight-line propagation. As can be seen from Fig. 8(d), although the increase of fourth-order dispersion coefficient enhances the tunneling strength, it can be clearly observed that the effect of fourth-order dispersion is much weaker compared with the increase of second-order. Figure 8(f) shows the evolution of the soliton when the third-order dispersion coefficient increases, the tunneling phenomenon is obviously
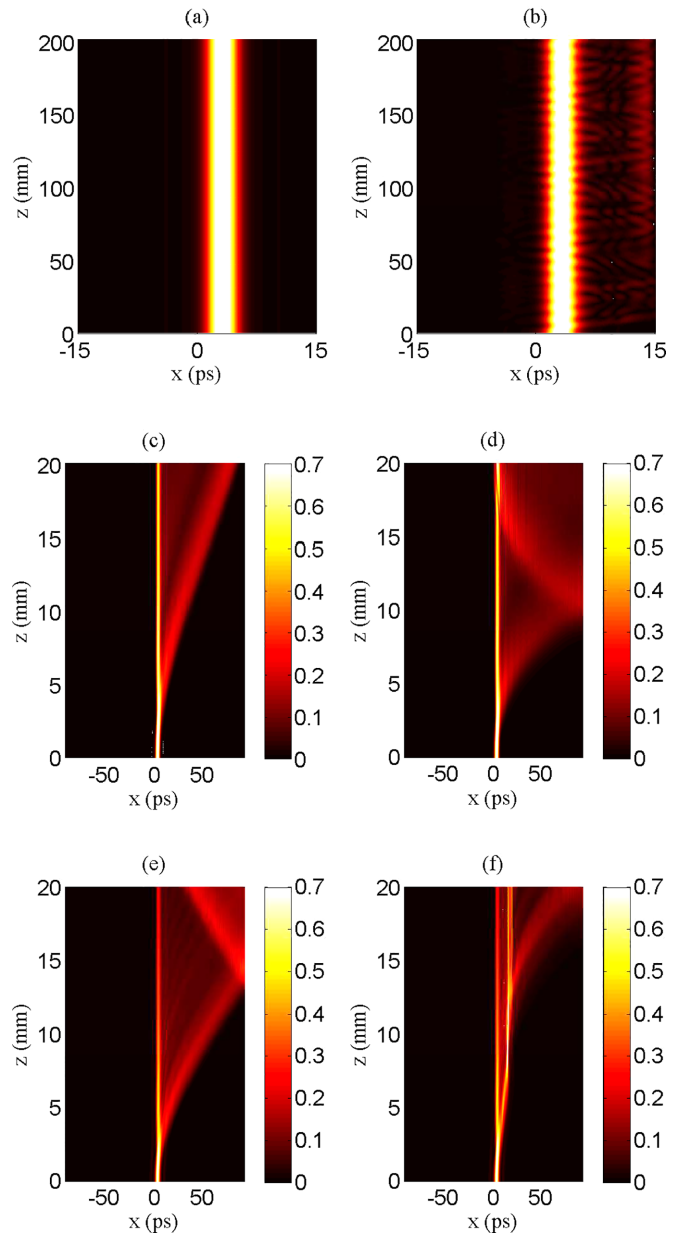
FIG. 8. Real-time evolutionary results of solitons for $c = v_0 = 1$ in the first gap which is $\mu = 0$ and the color is expressed as $|\phi(x)|$. (a)–(c) have the same dispersion coefficient $\beta_2 = 1$, $\beta_3 = 0$, $\beta_4 = 0$ and strength of different transverse biases β. (a) Stable propagation for $\beta = 0$. (b) Bloch oscillation for $\beta = 0.1$. (c) Optical tunneling for $\beta = 0.5$. (d) Optical tunneling for $\beta = 0.5$, $\beta_2 = 1$, $\beta_3 = 0$, and $\beta_4 = 1$. (e,f) differ only in third-order dispersion coefficients which have $\beta_3 = 0$ and 1, respectively. The other identical parameters are $\beta_2 = 2$, $\beta_4 = 0$, and $\beta = 0.5$.

suppressed. Although the tunneling intensity almost does not change, it is mainly concentrated near the main soliton wave. The monitoring results are consistent with the previous findings.

VI. CONCLUSION

In summary, we studied the nonlinear LZSM tunneling under higher-order dispersion, given the law of variation of

the loop structure by analyzing the fixed points of the classical Hamiltonian, and systematically discussed the effect of the dispersion term on the loop structure and tunneling probability. Our results showed that the effect of second- and fourth-order dispersion on tunneling was the same, except that fourth-order dispersion affects it to a lesser extent than second-order dispersion. We gave exact values for the linear case, in agreement with the simulations. However, when third-order dispersion was present, it dramatically affected the tunneling, breaking the loop structure's symmetry and leading to nonreciprocal LZSM tunneling. In the end, we gave the real-time evolution of solitons under transverse bias, which gave consistent results by comparison with the laws of the nonlinear two-energy level model. The findings in the present work have enriched our alternative understanding of the loop structure and nonlinear LZSM tunneling.

[1] J. Liu, L. Fu, B.-Y. Ou, S.-G. Chen, D.-I. Choi, B. Wu, and Q. Niu, Theory of nonlinear Landau-Zener tunneling, Phys. Rev. A **66**, 023404 (2002).

[2] B. Wu and Q. Niu, Nonlinear Landau-Zener tunneling, Phys. Rev. A **61**, 023402 (2000).

[3] Y. Zhang, Z. Chen, B. Wu, T. Busch, and V. V. Konotop, Asymmetric Loop Spectra and Unbroken Phase Protection Due to Nonlinearities in $\mathcal{PT}$-Symmetric Periodic Potentials, Phys. Rev. Lett. **127**, 034101 (2021).

[4] B. Prasanna Venkatesh, J. Larson, and D. H. J. O'Dell, Band-structure loops and multistability in cavity qed, Phys. Rev. A **83**, 063606 (2011).

[5] D. Diakonov, L. M. Jensen, C. J. Pethick, and H. Smith, Loop structure of the lowest Bloch band for a Bose-Einstein condensate, Phys. Rev. A **66**, 013604 (2002).

[6] Q. Guan, M. K. H. Ome, T. M. Bersano, S. Mossman, P. Engels, and D. Blume, Nonexponential Tunneling due to Mean-Field-Induced Swallowtails, Phys. Rev. Lett. **125**, 213401 (2020).

[7] Z. Huang and Y. Zhao, Dynamics of dissipative Landau-Zener transitions, Phys. Rev. A **97**, 013803 (2018).

[8] D. M. Di Paola, M. Kesaria, O. Makarovsky, A. Velichko, L. Eaves, N. Mori, A. Krier, and A. Patanè, Resonant Zener tunnelling via zero-dimensional states in a narrow gap diode, Sci. Rep. **6**, 32039 (2016).

[9] R. Khomeriki, Nonlinear Landau-Zener tunneling in coupled waveguide arrays, Phys. Rev. A **82**, 013839 (2010).

[10] V. Loladze and R. Khomeriki, Landau-Zener tunneling of solitons, Phys. Rev. E **95**, 042204 (2017).

[11] R. Khomeriki, L. Chotorlishvili, and J. Berakdar, Landau-Zener tunneling in multiferroic composites, New J. Phys. **17**, 013030 (2015).

[12] N. A. Sinitsyn, Landau-Zener transitions in chains, Phys. Rev. A **87**, 032701 (2013).

[13] O. V. Ivakhnenko, S. N. Shevchenko, and F. Nori, Nonadiabatic Landau-Zener-Stückelberg-Majorana transitions, dynamics, and interference, Phys. Rep. **995**, 1 (2023).

[14] S. Ashhab, O. A. Ilinskaya, and S. N. Shevchenko, Nonlinear Landau-Zener-Stückelberg-Majorana problem, Phys. Rev. A **106**, 062613 (2022).

[15] F. Wilczek, Majorana and condensed matter physics, arXiv:1404.0637.

[16] P. Kofman, O. V. Ivakhnenko, S. N. Shevchenko, and F. Nori, Majorana's approach to nonadiabatic transitions validates the adiabatic-impulse approximation, arXiv:2208.00481.

[17] Y. B. Band and Y. Avishai, Three-level Landau-Zener dynamics, Phys. Rev. A **99**, 032112 (2019).

[18] Y. Zhang, Z. Gui, and Y. Chen, Nonlinear dynamics of a spin-orbit-coupled Bose-Einstein condensate, Phys. Rev. A **99**, 023616 (2019).

[19] A. Blanco-Redondo, C. M. de Sterke, J. E. Sipe, T. F. Krauss, B. J. Eggleton, and C. Husko, Pure-quartic solitons, Nat. Commun. **7**, 10427 (2016).

[20] A. F. J. Runge, D. D. Hudson, K. K. K. Tam, C. M. de Sterke, and A. Blanco-Redondo, The pure-quartic soliton laser, Nat. Photonics **14**, 492 (2020).

[21] K. K. K. Tam, T. J. Alexander, A. Blanco-Redondo, and C. M. de Sterke, Generalized dispersion Kerr solitons, Phys. Rev. A **101**, 043822 (2020).

[22] E. N. Tsoy and C. M. de Sterke, Theoretical analysis of the self-frequency shift near zero-dispersion points: Soliton spectral tunneling, Phys. Rev. A **76**, 043804 (2007).

[23] V. I. Kruglov and H. Triki, Quartic and dipole solitons in a highly dispersive optical waveguide with self-steepening nonlinearity and varying parameters, Phys. Rev. A **102**, 043509 (2020).

[24] H. Triki and V. I. Kruglov, Propagation of dipole solitons in inhomogeneous highly dispersive optical-fiber media, Phys. Rev. E **101**, 042220 (2020).

[25] V. S. Shchesnovich, S. B. Cavalcanti, J. M. Hickmann, and Y. S. Kivshar, Zener tunneling in two-dimensional photonic lattices, Phys. Rev. E **74**, 056602 (2006).

[26] A. S. Desyatnikov, Y. S. Kivshar, V. S. Shchesnovich, S. B. Cavalcanti, and J. M. Hickmann, Resonant Zener tunneling in two-dimensional periodic photonic lattices, Opt. Lett. **32**, 325 (2007).

[27] S. Kitamura, N. Nagaosa, and T. Morimoto, Nonreciprocal Landau–Zener tunneling, Commun. Phys. **3**, 63 (2020).

[28] J. Liu, B. Wu, and Q. Niu, Nonlinear Evolution of Quantum States in the Adiabatic Regime, Phys. Rev. Lett. **90**, 170404 (2003).

[29] A. Smerzi, S. Fantoni, S. Giovanazzi, and S. R. Shenoy, Quantum Coherent Atomic Tunneling between Two Trapped Bose-Einstein Condensates, Phys. Rev. Lett. **79**, 4950 (1997).

[30] G.-F. Wang, D.-F. Ye, L.-B. Fu, X.-Z. Chen, and J. Liu, Landau-Zener tunneling in a nonlinear three-level system, Phys. Rev. A **74**, 033414 (2006).

[31] X. Xu, Z. Zhang, and Z. Liang, Nonequilibrium Landau-Zener tunneling in exciton-polariton condensates, Phys. Rev. A **102**, 033317 (2020).

[32] I. Y. Chestnov, A. V. Yulin, A. P. Alodjants, and O. A. Egorov, Nonlinear Bloch waves and current states of exciton-polariton condensates, Phys. Rev. B **94**, 094306 (2016).

[33] Y. B. Band, B. Malomed, and M. Trippenbach, Adiabaticity in nonlinear quantum dynamics: Bose-Einstein condensate in a time-varying box, Phys. Rev. A **65**, 033607 (2002).

[34] C. Zener, Non-adiabatic crossing of energy levels, Proc. Math. Phys. Eng. Sci **137**, 696 (1932).

[35] L. D. Landau, Zur Theorie der Energieubertragung II, Z. Sowjetunion **2**, 46 (1932).

[36] J. Yang and T. I. Lakoba, Universally-convergent squared-operator iteration methods for solitary waves in general nonlinear wave equations, Stud. Appl. Math. **118**, 153 (2007).

[37] S. Yu, S. Zhao, and G. Wei, Local spectral time splitting method for first- and second-order partial differential equations, J. Comput. Phys. **206**, 727 (2005).

[38] Z. Cao, X. Li, Q. Tan, W. Jiang, D. Liang, and J. Dou, Trajectory variations of optical Bloch oscillations for Airy beams in transversely and longitudinally modulated photonic lattices, Appl. Opt. **56**, 3484 (2017).

[39] P. He and Z. Li, Nonlinear Bloch-Zener oscillations for Bose-Einstein condensates in a Lieb optical lattice, New J. Phys. **22**, 063031 (2020).

[40] F. K. Abdullaev, B. B. Baizakov, S. A. Darmanyan, V. V. Konotop, and M. Salerno, Nonlinear excitations in arrays of Bose-Einstein condensates, Phys. Rev. A **64**, 043606 (2001).

[41] Y. Zhang, R. Wang, H. Zhong, J. Zhang, M. R. Belić, and Y. Zhang, Optical Bloch oscillation and Zener tunneling in the fractional Schrödinger equation, Sci. Rep. **7**, 17872 (2017).